***JKPK (JURNAL KIMIA DAN PENDIDIKAN KIMIA)**, Vol. 10, No.1, 2025* — *pp. 132-153*
Chemistry Education Study Program, Universitas Sebelas Maret — *ISSN 2503-4146*
https://jurnal.uns.ac.id/jkpk — *ISSN 2503-4154 (online)*

Removal of Cu(II) and Pb(II) Ions from Wastewater Solutions Using Black Soldier Fly (*Hermetia illucens*) Pupal Shell: Adsorption and Characterization

Eko Prasetyo Kuncoro[1*], Azra Rhea Darmawati[1], Pramudya Lizza Roshita[1], Thin Soedarti[2]

[1]*Environmental Engineering, Department of Biology, Faculty of Science and Tecnology, Universitas Airlangga, Surabaya, Indonesia*
[2]*Department of Biology, Faculty of Science and Tecnology, Universitas Airlangga, Surabaya, Indonesia*

ARTICLE INFO

Keywords:
Clean Water;
Hermetia Illucens*;*
Heavy Metals;
Removal;
Adsorption.

Article History:
Received: 2025-03-05
Accepted: 2025-04-13
Published: 2025-04-30
*d*oi:10.20961/jkpk.v10i1.100111

ABSTRACT

Industrial wastewater often contains heavy metals such as Pb(II) and Cu(II) that pose significant environmental and health risks. This study investigates the utilization of Black Soldier Fly (BSF) (*Hermetia illucens*) pupal shells as an adsorbent material for the removal of Pb(II) and Cu(II) ions from aqueous solutions. BSF pupal shells were chosen due to their high availability, rapid life cycle, and chitin-rich composition, making them suitable for heavy metal adsorption. The preparation process included washing, drying, grinding, and activation with 1 M NaOH solution. Characterization of the adsorbent was performed before and after adsorption using Fourier Transform Infrared Spectroscopy (FTIR) and Scanning Electron Microscopy coupled with Energy Dispersive X-ray Spectroscopy (SEM-EDX). Adsorption experiments were conducted to examine the effects of pH, contact time, and initial ion concentration. The optimum pH for adsorption was found to be 5.5, achieving removal efficiencies of 95.5% for Pb(II) and 71.81% for Cu(II). The optimum contact times were 180 minutes for Pb(II) and 240 minutes for Cu(II). Kinetic analysis demonstrated that the adsorption process followed a pseudo-second-order model. Adsorption isotherm studies indicated that the Langmuir model provided a better fit (R^2 = 0.99 for Pb(II) and 0.98 for Cu(II)) compared to the Freundlich model (R^2 = 0.90 for Pb(II) and 0.77 for Cu(II)). These results demonstrate that BSF pupal shells are a promising, cost-effective, and environmentally friendly material for industrial wastewater treatment applications

**Corresponding Author:* *eko-p-k@fst.unair.ac.id*

How to cite: E. P. Kuncoro, A. R., Darmawati, P. L. Roshita, T. Soedarti, "Removal of Cu(II) and Pb(II) Ions from Wastewater Solutions Using Black Soldier Fly (*Hermetia illucens*) Pupal Shell: Adsorption and Characterization," *Jurnal Kimia dan Pendidikan Kimia (JKPK)*, vol. 10, no. 1, pp. 132–152, 2025. [Online]. Available: http://dx.doi.org/10.20961/jkpk.v10i1.100111

INTRODUCTION

The manufacturing industry in Indonesia has been increasing and it is estimated that the growth rate would reach 20% by 2023, according to the Indonesian Ministry of Industry. Manufacturing activities include textile, metal processing, wood processing, leather tanning, fertilizer production, and metal plating industries. The growing community demand for industrial goods stimulates the development of electroplating industries in Indonesia. However, most small-scale industries lack adequate wastewater treatment facilities, resulting in direct discharge of their wastewater into rivers or sewage canals, leading to environmental pollution. Recent research has confirmed that Indonesian waters are polluted with heavy metals such as Pb, Cu, Cd, Al, and Fe [1], [2]. With the continuous development of the electroplating industry, an increasing amount of hazardous waste, including heavy metal wastewater, is generated. Industrial wastewater may contain dangerous pollutants such as heavy metals (cadmium, lead, copper, chromium), organic compounds, oils and fats, acids (sulfate, nitrate), pesticides, phosphates, and chlorides. For instance, a study of domesticated wastewater samples in East Java revealed lead (39.55 mg/L), iron (28.10 mg/L), copper (49.85 mg/L), cadmium (31.65 mg/L), zinc (8.21 mg/L), and nickel (14.82 mg/L), far exceeding WHO permissible limits (e.g., 0.05 mg/L for lead). Such waste is highly toxic, corrosive, and environmentally hazardous to human health [3].

To meet water quality standards, wastewater containing heavy metals must be treated before discharge. Government regulations specify permissible discharge levels of 0.03–0.5 mg/L for lead and 0.02–0.2 mg/L for copper (PP No. 22 Tahun 2021). Common heavy metal treatment methods include chemical reduction, precipitation, ion exchange, membrane separation, solvent extraction, adsorption, and biological methods, each presenting drawbacks such as high energy demand, heavy chemical usage, or high cost [4]. Reverse osmosis and electrodialysis, while effective, are expensive and limited in certain applications such as arsenic removal [5], [6]. Other methods like solvent extraction and bioremediation are also cost-prohibitive for small-scale systems [7]. Adsorption emerges as an effective, efficient, and low-cost technology, widely used for removing heavy metals and organic matter from wastewater without producing toxic byproducts.

Adsorption involves the adherence of one substance (adsorbate) onto the surface of another (adsorbent). Materials such as activated carbon, zeolite, clay, and natural polymers from animal shells have been explored as nontoxic adsorbents [8], [9]. One promising adsorbent is Black Soldier Fly (BSF) (*Hermetia illucens*) pupal shells, which in Indonesia generate 30–400 kg/day of waste from BSF farming activities, mostly unmanaged [10]. Efficient utilization of this waste aligns with the circular economy principles, promoting resource optimization and waste minimization.

BSF pupal shells are primarily composed of 40–50% chitin, proteins, cellulose, and trace lignin. Chitin, a natural polymer of N-acetylglucosamine, provides polar functional groups facilitating interactions with metal ions, proteins, and organic compounds [11]. The calcium, phosphorus, and magnesium content in the shell also enhances its structural integrity and adsorption capacity. Previous studies reported variations in chitin content from BSF pupal shells (8%, 12.4%, 85%) depending on the extraction process [12]–[14].

Chitin has been extensively used as an adsorbent for heavy metals due to its low cost and high adsorption efficiency. For instance, chitin from red shrimp (*Solenocera melantho*) achieved 99.7% Pb removal [16], while shrimp shell chitin demonstrated 270.27 mg/g zinc adsorption capacity [17], and yellow lobster chitin achieved 58 mg/g Cu adsorption [18]. BSF pupal shells, containing both chitin and calcium carbonate, have also shown potential for dye removal, achieving 99% removal efficiency for bromophenol blue at pH 4 with 20 mg of adsorbent [19]. However, studies on heavy metal adsorption by BSF pupal shells remain limited.

Thus, this study was conducted to evaluate the properties, functional groups, and adsorption capacities of BSF pupal shells for Pb(II), Cu(II), and Cr(VI) removal under various pH, contact time, and initial metal concentrations. Characterization was performed using pHpzc analysis, Fourier Transform Infrared Spectroscopy (FTIR), and Scanning Electron Microscopy–Energy Dispersive X-ray Spectroscopy (SEM-EDX). It is anticipated that the findings will contribute to the development of cost-effective and environmentally sustainable wastewater treatment technologies.

METHODS

1. Equipment and materials

The equipment used in this research included a 40 mesh sieve, blender, pipette dropper, spatula, porcelain crucible, porcelain cup, mortar and pestle, 100 mL glass bottle, oven, pH meter, analytical balance, filter paper, 25 mL measuring glass, 1000 mL and 500 mL volumetric flask, 1000 mL and 100 mL beaker glass, filter paper, Buchner funnel, Buchner flask, vacuum pump, shaker, 100 mL plastic sample bottle, Shimadzu AA-700, and Thermo Scientific Nicolet iS10 equipped with FTIR. The materials used in this research included Black Soldier Fly pupal shell, destilled water, Pb(II) solution, Cu(II) solution, 1 N NaOH solution, 1 M HCl solution,and 0.1 M NaCl solution.

2. Preparation of Black Soldier Fly (*Hermetia illucens*) Pupal Shell Adsorbent

A sample of 1.5 kg of Black Soldier Fly pupal shell was washed with running water, followed by rinsing with destilled water to ensure cleanliness. The cleaned BSF pupal shell was then dried in an oven at 60°C until a constant mass was achieved to eliminate moisture, facilitating the subsequent grinding process. Once dried, the sample was ground using a pestle and mortar, followed by sieving through a 40 mesh sieve. The sample obtained was activated using 1 M NaOH.

Activation of adsorbent involved placing 100 g of the sample in a 1000 mL beaker and adding 500 mL of 1 M NaOH solution until the sample was submerged. The selection of 1 M NaOH was based on previous research and preliminary tests conducted previously [20]. Preliminary tests conducted without activation resulted in low removal efficiency. The sample was soaked in the NaOH solution for 24 hours. After soaking, the sample was filtered to separate it from the solution. Subsequently, it was washed with destilled water until reaching a neutral pH. Finally, the activated sample was dried in an oven at 60°C until a constant mass of the adsorbent was achieved [21].

3. Adsorption Studies

The study aimed to determine optimal conditions for Pb(II) and Cu(II) ion adsorption efficiency through variations in pH, contact time, and concentration. Various pH levels (2, 3, 4, 5, 5.5, 6, and original pH) were tested by adjusting synthetic metal solutions to these pH levels using 1 M HCl or NaOH. The use of synthetic wastewater prior to real wastewater was chosen because this research was the first step to examine the ability of material toward single metal adsorption. For further research, real wastewater would be used for mixed multi metals. To study the effect of pH, solutions contained 40 mg/L of Pb(II) and Cu(II), with 1 g of adsorbent added. The solutions were shaking at 240 rpm for 180 minutes at room temperature followed by settling for 1 minute preceded filtration and then analyzed using AAS. To study the effet of contact time: 5, 10, 15, 30, 60, 90, 120, 150, 180, 210, and 240 minutes of contact time were tested after adjusting 100 mL synthetic metal solutions to optimal pH. To study the effect of metal concentration, experiments were carried out using metal concentration ranging from 5 to 150 mg/L under pH 5.5 condition. Solutions were prepared, adjusted, and treated similarly as in the pH and contact time studies, with subsequent AAS analysis. Each experiment was conducted in triplicate, ensuring robust data collection and analysis according to SNI 6989.9:2009 standards. The removal of Cu(II) and Pb(II) was calculated using the following equation:

$$Removal\ (\%) = \left(\frac{C_0 - C_e}{C_0}\right) x\ 100 \qquad (1)$$

where, C_0 is the initial concentration of metal ion (mg/L), C_e is the equilibrium concentration of metal ion (mg/L).

4. Characteristics of Adsorbent

The adsorbent was tested for its characteristics using several analytical methods. Firstly, the pHpzc test was conducted using the salt addition method with NaCl 0.01 M to determine the pHpzc value. NaCl solution was added to a beaker with the initial pH of the solution varied from 2 to 12 using 0.1 M NaOH and 0.1 M HCl. Subsequently, the solution was transferred to a glass bottle and homogenized with 1 g of BSF adsorbent for 24 hours at room temperature. The final pH of the solution was recorded and used to plot the pHpzc graph by comparing ΔpH (initial pH – final pH) against the initial pH [22]. Fourier Transform Infrared Spectroscopy (FTIR) was used to identify functional groups and chemical bonds of the BSF pupal shell before and after contact with Pb(II) and Cu(II) ions. A sample of 1 g was analyzed with FTIR using wavelengths ranging from 400 to 4000 cm^{-1}. SEM-EDX analysis was conducted to evaluate the surface morphology and elemental composition of the BSF adsorbent before and after exposure to heavy metals. These methods collectively provided a comprehensive understanding of the physicochemical properties of BSF adsorbents and their potential applications in wastewater treatment.

RESULTS AND DISCUSSION

1. pHpzc Analysis

The determination of pHpzc in this study was performed by varying the initial pH from 2, 3, 4, 5, 6, 7, 8, 9, 10, 11, and 12, resulting in final pH values of 8.9, 9.3, 9.3, 9.3, 9.4, 9.3, 9.4, 9.4, 9.5, 10.8, and 11.5, respectively. The ΔpH values (final pH – initial pH) were calculated and plotted against the initial pH to construct the graph shown in Figure 1.

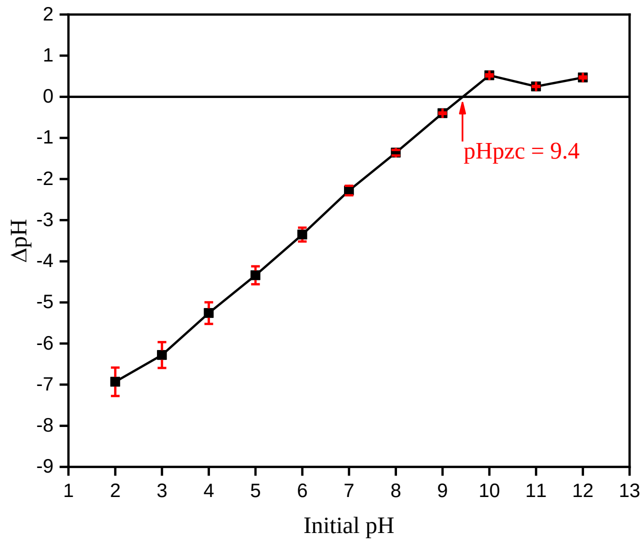

Figure 1. pHpzc of BSF pupal shell

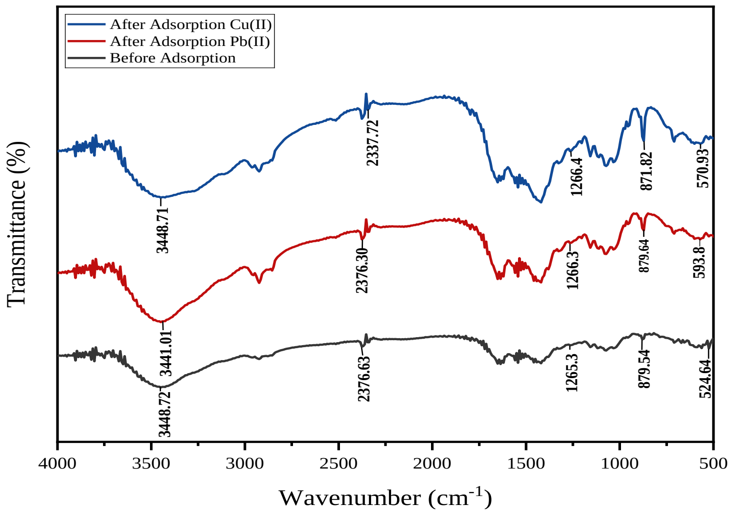

Figure 2. FTIR spectra of BSF pupal shell

The pHpzc value was determined as the point where the ΔpH curve crosses the x-axis (ΔpH ≈ 0). Based on Figure 1, the pHpzc of the Black Soldier Fly (BSF) pupal shell adsorbent was found to be 9.4. This indicates the pH at which the surface charge of the adsorbent is neutral, with an equal number of positive and negative charges. Below the pHpzc, the adsorbent surface becomes positively charged, while above the pHpzc, the surface becomes negatively charged [23].

Although pHpzc provides important information, adsorption efficiency is influenced by multiple factors beyond surface charge alone [24]. At certain pH levels, precipitation of metal ions can occur, affecting the observed adsorption independently of electrostatic interactions. Specifically, for Pb(II) and Cu(II) ions, precipitation may occur at pH values lower than the pHpzc, thus limiting the accuracy of using pHpzc alone to determine the optimal pH for adsorption. Nevertheless, a high pHpzc value suggests that the BSF pupal shell is highly basic, with abundant surface hydroxyl groups (–OH) favorable for cationic heavy metal adsorption.

2. FTIR Analysis

Fourier Transform Infrared (FTIR) spectroscopy was utilized to characterize the functional groups present on the surface of the BSF (*Hermetia illucens*) pupal shell adsorbent before and after Pb(II) and Cu(II) adsorption, as shown in Figure 2.

The FTIR in Figure 2, with various insets, has peaks at different wavenumbers such that functional groups in the adsorbent can be also determined. It can be seen that the peak observed at 3448.72 cm^{-1}, 3448.71 cm^{-1}, and the peak at 3441.01 cm^{-1} reflect O–H and N–H bond functional groups [25]. The peak read when the adsorbent adsorbs Cu(II) is displaced at 2337.72; 2376.30; and 2376.63 cm^{-1} that corresponds to C≡C functional group, respectively. The next optimal conditions appear around 1266.3 cm^{-1}, 1266.4 cm^{-1}, and 1265.3 cm^{-1} corresponding to the characteristic C=N and C=C bands of the adsorbent.

The pre- and post-adsorbed peaks at wave numbers 879.54 cm^{-1}, 871.82 cm^{-1}, and 879.64 cm^{-1}, respectively, suggest the vibration of CO_3^{2-} functional group which is in the range of wave number 712–1427 cm^{-1}. The CO_3^{2-} vibrational functional group was indicative of the $CaCO_3$ compounds and were detected from the BSF pupal shell adsorbent [26]. The peak at wave number 524.24 cm^{-1} before adsorption indicates the presence of C–H. The peak then grows in the Cu adsorption stage at wave number 570.93 cm^{-1} implying the presence of Cu–O bonds. The presence of the Cu–O bond implies a combination between Cu(II) and functional groups of the BSF pupal shell adsorbent. The Cu–O bond into the adsorbent is in stretching vibrations [20]–[24], and the Cu–O bond could be identified at the wave numbers in the range of 525–584 cm^{-1} [27].

From the obtained analysis, it can be observed that the FTIR curve is displaying binding of ions which is engaged with the functional groups available in the adsorbent. This shift in wave number is due to the O–H, N–H, C≡C, C=N, C=C, CO_3^{2-}, C–H, and Cu–O functional groups. From this it can be deduced that adsorption by BSF (*Hermetia illucens*) pupal shell can take place because of the existence of chitin that consists of functional groups O–H, N–H, C–H, and C–N, and $CaCO_3$ compounds on the adsorbent, that are marked by the existence of CO_3^{2-} cognate group. FTIR results are given in Table 1 and 2 below

Table 1. Result of FTIR before and after Pb adsorption.

Wavenumber before adsorption (cm^{-1})	Wavenumber after adsorption Pb(II) (cm^{-1})	∆Wavenumber (cm^{-1})
3448.72	3441.01	7.71
2376.63	2376.30	0.33
1265.3	1266.3	1
879.54	879.64	0.1
524.64	593.8	69.16

Table 2. Result of FTIR before and after Cu adsorption.

Wavenumber before adsorption (cm^{-1})	Wavenumber after adsorption Cu(II) (cm^{-1})	∆Wavenumber (cm^{-1})
3448.72	3448.71	0.01
2376.63	2337.72	38.91
1265.3	1266.4	1.1
879.54	871.82	7.72
524.64	570.93	46.29

3. SEM-EDX Analysis

The morphology of the BSF pupal shell was studied to characterize the adsorbent using Scanning Electron Microscope (SEM). In EDX analysis, however, only the elements in the adsorbent are analyzed for their composition. SEM investigation in the study was carried out before and after the adsorption of Pb(II) and Cu(II) to determine the changes in surface morphology and elemental composition of the adsorbent. The SEM (10,000×) was used to observe the surface morphology of the adsorbent. SEM images are shown in Figure 3.

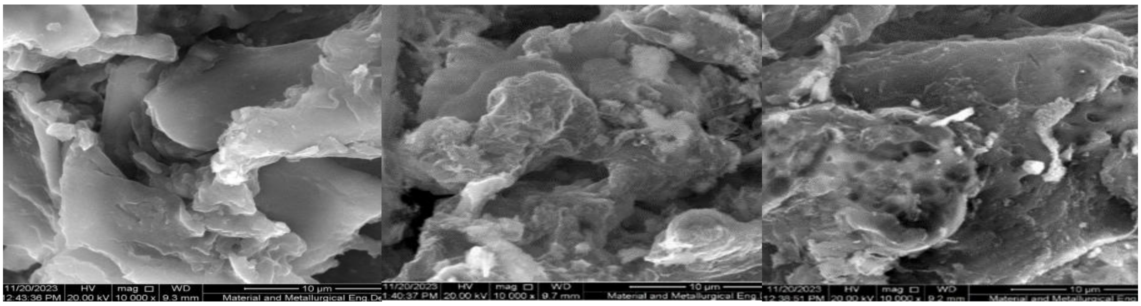

a b c

Figure 3. SEM analysis of the adsorbent before adsorption (a), after Pb(II) adsorption (b), after Cu(II) adsorption (c).

The surface morphology of the adsorbent was rugged and uneven before adsorption. Nevertheless, the surface structure became denser and more compact after adsorption of heavy metals. This effect is explained by the interaction of the adsorbent and the adsorbate, such that the rough surface of the adsorbent is occupied by metallic ions attached thereto. SEM images revealed a repetitive hexagonal microfibril network which looks like a honeycomb on the surface of the adsorbent. This is in line with other studies [28], where it was reported that Black Soldier Fly (*Hermetia illucens*) pupal shell chitosan contains a hexagonal microfibril structure, akin to a honeycomb. SEM observation revealed a honeycomb-like hexagonal microfibril repeating unit on the surface of the adsorbent. This is consistent with the results of another study [29], which demonstrated that the chitosan microspheres derived from *Hermetia illucens* have a well-ordered hexagonal microfibril, similar to the honeycomb structure, increasing specific surface area, and average pore size [30].

EDX was used to give information on the adsorbent chemical composition in terms of distribution of the detected elements. The elemental mapping is shown in Figure 4.

EDX analysis in Figure 5 indicates the presence of Ca included in the BSF (*Hermetia illucens*) pupal shell adsorbent before adsorption of Pb(II). Pb–Ca interaction was achieved through the successful adsorption of Pb(II), and lead was observed on the adsorbent surface after Pb(II) adsorption. After exposure to Cu(II), EDX showed more Cu, demonstrating the interaction of adsorbent–adsorbate. Elemental compositions in Pb(II) and Cu(II) adsorbed and un-adsorbed states have been summarized from the EDX graphs (Figure 5), which is helpful for qualification of material, identification of pollutants, and mapping of elements.

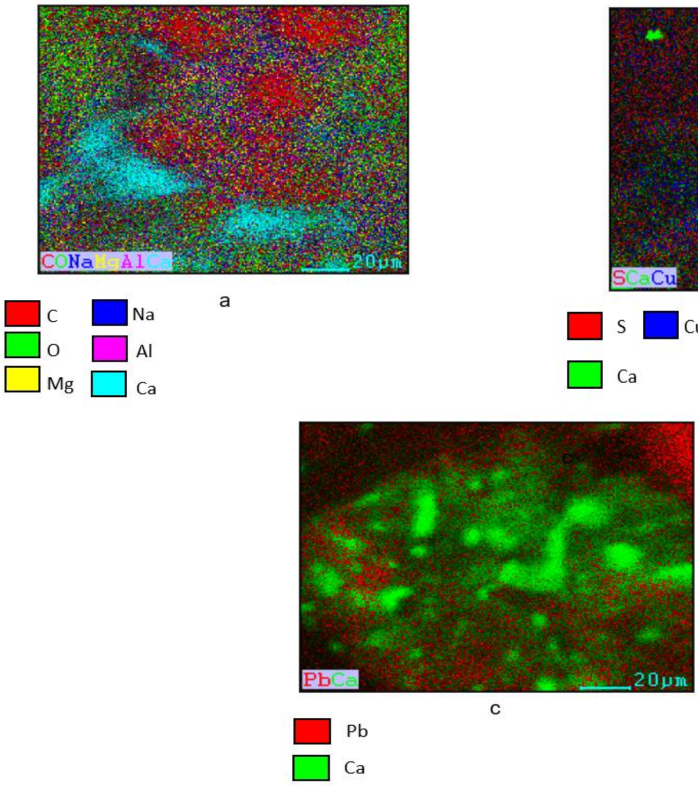

Figure 4. Composition of adsorbent elements before adsorption (a), after Pb(II) adsorption (b), after Cu(II) adsorption (c).

According to the EDX spectra (Figure 5), before Pb(II) and Cu(II) adsorption, the elemental composition of adsorbent was C, O, Na, Al, and Ca with ratios of 54.47%, 35.75%, 3.60%, 0.77%, and 4.06%, respectively. The elemental values of the adsorbent after removal of Pb(II) are C (22.13%), O (32.19%), Al (2.08%), Ca (34.75%), and Pb (5.24%). After the adsorption of Cu(II), the adsorbent was composed of C, O, Na, Al, Ca, and Cu, with mass fractions of 40.80% C, 31.78% O, 2.03% Na, 7.53% Al, 7.47% Ca, and 4.67% Cu. The presence of C, O, and Ca indicates that the $CaCO_3$ produced during Pb(II) adsorption is confirmed by FTIR. The reduction of Na after adsorption represents ion exchange. Al, as a contaminant of aluminum foil with which samples were stored, was also determined. The EDX analysis after adsorption showed that heavy metals Pb and Cu from synthetic wastewater were largely adsorbed onto the adsorbent surface. The alteration in elemental composition of the adsorbent before and after adsorption may be attributed to complexes formed between metal ions and functional groups in the adsorbent pores resulting from foreign exchange, which may have changed the elemental contents or formed new composites.

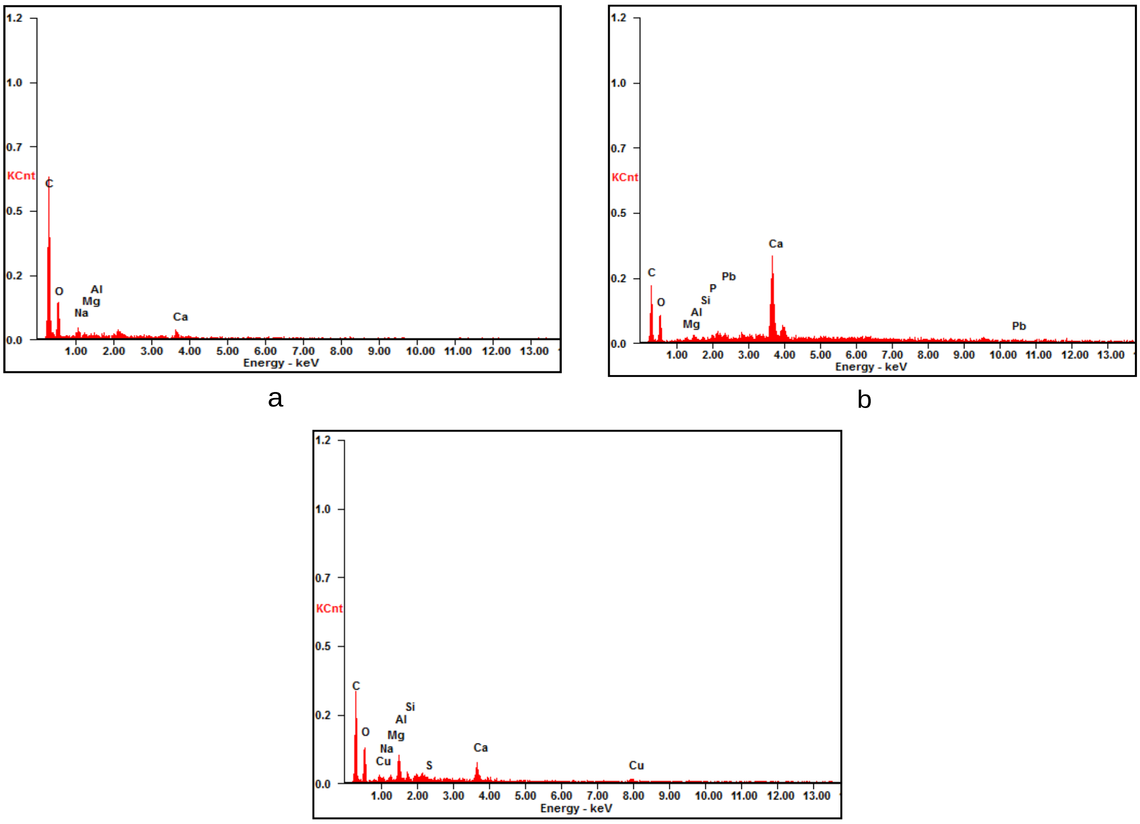

Figure 5. EDX analysis of adsorbent before adsorption (a), after Pb(II) adsorption (b), after Cu(II) adsorption (c)

4. Effect of pH

The pH or acidity level is a crucial factor in the adsorption of heavy metal ions because it influences the protonation of active sites on the adsorbent molecules, thereby affecting the surface charge of the adsorbent and ionization degree. Generally, at low pH conditions, heavy metal ions compete with hydrogen ions to bind to the active sites of the adsorbent, whereas at high pH, heavy metal ions may precipitate out. The efficiency of Pb(II) and Cu(II) adsorption at different pH levels is illustrated in Figure 6.

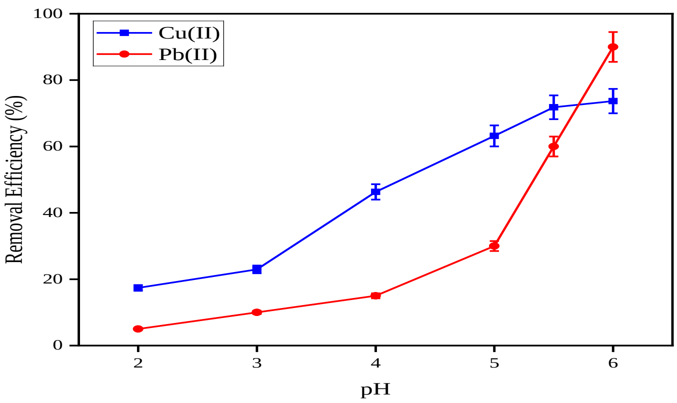

Figure 6. Removal Efficiency based on pH variation.

Based on the graph, it can be observed that the lowest efficiency of Pb(II) adsorption occurs at pH 2, with 12.30%, while the highest efficiency is at pH 5.5, reaching 95.5%. Similarly, the efficiency of Cu(II) adsorption is 17.38% at pH 2 and 72.55% at pH 6. This indicates that adsorption efficiency tends to increase with higher pH of the solution. The lower adsorption of metal ions in acidic pH solutions is due to the higher concentration of H^+ ions on the adsorbent surface, leading to competition between H^+ ions and metal ions for interaction with active sites on the adsorbent. Conversely, higher metal ion adsorption at basic pH is attributed to the decreasing concentration of H^+ ions, allowing more active sites on the adsorbent to adsorb heavy metal ions.

Determination of the optimum pH for adsorption of Pb(II) and Cu(II) using BSF pupal shell adsorbent is based on consideration of the highest efficiency value, statistical analysis, and pH of precipitation. Determination of the optimum pH for adsorption of Pb(II) and Cu(II) in this study is pH 5.5. pH 5.5 was chosen because it shows a high value of adsorption efficiency and is below the pH of precipitation. At pH 5.5, the adsorption efficiency for Pb(II) was 95.5% and for Cu(II) was 71.81%. Cu removal efficiency is lower than Pb due to the pH factor of precipitation or deposition. Pb and Cu has a precipitation pH of 5.94 and 5.77. Cu metal at pH 5.5 is almost close to the precipitation pH, so the adsorbent's ability to adsorb is less strong [31].

5. Effect of Contact Time

Research on contact time indicates that the adsorption rate of metal ions increases with time until reaching an optimum value. The efficiency of Pb(II) and Cu(II) adsorption at each contact time is illustrated in Figure 7.

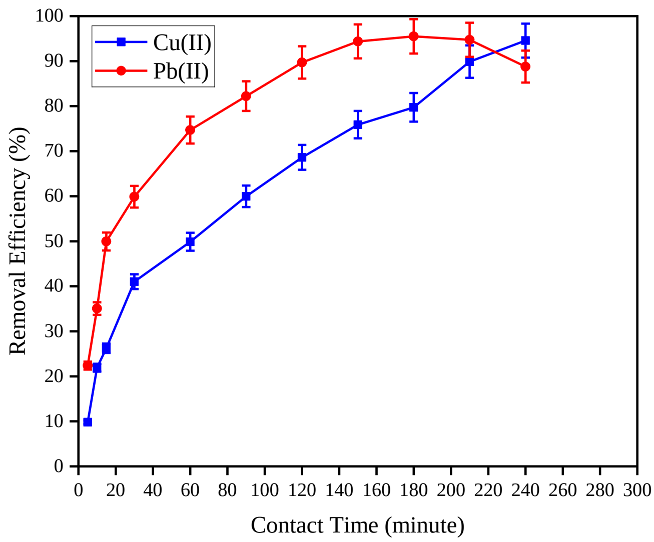

Figure 7. Removal Efficiency based on contact time.

According to the Figure 7, the lowest efficiency of Pb(II) adsorption occurs at 5 minutes (22.38%), and the highest efficiency is observed at 180 minutes (95.50%).

Similarly, for Cu(II), the lowest efficiency is at 5 minutes (9.81%), and the highest is at 240 minutes (94.56%). This indicates that longer interaction between the adsorbent and the solution leads to more metal ions being trapped. However, the active sites on the adsorbent gradually decrease during initial adsorption, resulting in a decline in the amount of metal ions adsorbed. Additionally, prolonged contact time may lead to instability in the bond between the adsorbent and metal ions, causing some of the already adsorbed metal ions to desorb. The determination of the optimum contact time for Pb(II) adsorption using BSF pupal shell adsorbent *(Hermetia illucens*) was based on achieving the highest efficiency and statitical analysis. The optimum contact time determined in this study for Pb(II) adsorption was 180 minutes, while for Cu(II), it was 240 minutes.

240 minutes is a long time, for practical use, the higher mass of the adsorbent can be used. This provides more active sites in the surface of the adsorbent so contact time can be reduced. The selection of these optimum contact times was due to achieving adsorption equilibrium or no significant increase in adsorption.

6. Effect of Metal Concentration

The initial concentration of heavy metals in the solution is a crucial parameter influencing mass transfer between the solution and adsorbent, determining the adsorption efficiency. The initial concentrations varied in this study were 5 mg/L, 10 mg/L, 20 mg/L, 40 mg/L, 80 mg/L, 100 mg/L, 120 mg/L, and 150 mg/L. The study was conducted at pH 5.5 with an adsorbent dose of 1 g and an agitation speed of 240 rpm over 240 minutes. The impact of initial concentrations of Pb(II) and Cu(II) can be observed in Figure 8.

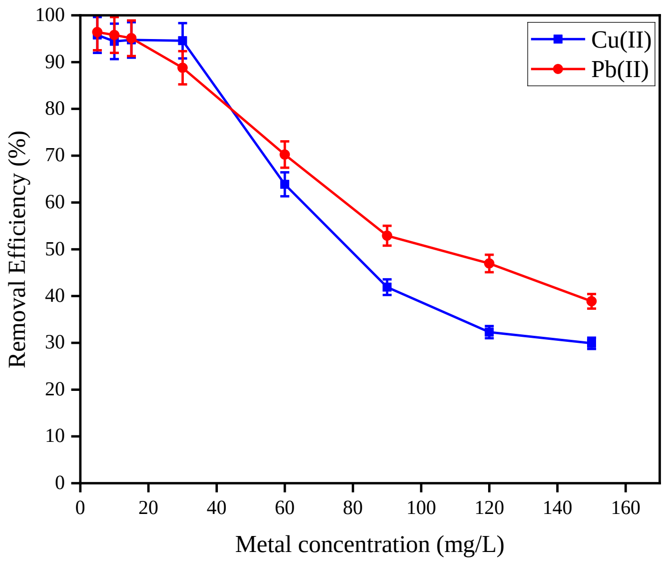

Figure 8. Removal Efficiency based on Concentration

The research results indicate that the highest Pb(II) adsorption efficiency was observed at an initial concentration of 20 mg/L, reaching 95.10%, which then gradually decreased to 38.87%. A similar trend was observed for Cu(II) adsorption, where the highest efficiency occurred at an initial concentration of 40 mg/L, achieving 94.56%, and decreased to 29.9% at an initial concentration of 150 mg/L. The increased adsorption at lower concentrations is due to available pristine active sites on the adsorbent, whereas at higher concentrations, adsorption sites become saturated, resulting in fewer metal ions being adsorbed. Based on these results, the optimum Pb(II) adsorption efficiency in this study was 95.10% at an initial concentration of 20 mg/L with adsorption capacity 19.2 mg/g, and the optimum Cu(II) adsorption efficiency was 94.56% at an initial concentration of 40 mg/L with adsorption capacity of 37.82 mg/g. Another study using the exoskeleton of BSF to remove Pb (II) metal also produced an adsorption capacity of 1.2 mg/g [32]. In addition, research on chitin can also adsorp Cu metal with a maximum adsorption capacity of 58 mg/g [19].

7. Adsorption Isotherm Model

The determination of adsorption isotherms is conducted to ascertain the adsorption capacity of an adsorbent towards an adsorbate. To determine the amount of adsorbate adsorbed onto the adsorbent, an equilibrium adsorption isotherm is required to derive the adsorption equation. Data in adsorption equilibrium are represented by adsorption isotherms that describe the relationship between the amount of adsorbate adsorbed per unit of adsorbent (qe) and the adsorbate concentration in the solution (Ce). In this study, adsorption isotherms were determined using the Langmuir and Freundlich models.

The Langmuir isotherm, the most fundamental model, assumes that metal ions form a single layer on the adsorbent surface where all sites have equal energy. When all sites are occupied, maximum adsorption occurs, preventing further metal binding. The Langmuir equation is linearized as:

$$\frac{C_e}{q_e} = \frac{C_e}{Q} + \frac{1}{Q_b} \qquad (2)$$

Where Q is the maximum adsorption at monolayer (mg/g), Ce is the equilibrium concentration of metal ion (mg/L), qe is the amount of metal ion adsorbed per unit weight of adsorbent at equilibrium concentration (mg/g), and b is the Langmuir constant related to the affinity of binding sites (mL/mg) and is a measure of the energy of adsorption. The Q and b can be determined from linear plot of Ce/qe against Ce.

The Freundlich isotherm model is typically employed to characterize adsorption on surfaces that are heterogeneous and capable of forming multiple layers. In this model, the initial adsorption involves the occupation of stronger binding sites by metal ions. As more sites become occupied, the overall binding strength tends to diminish. The linearized form of the Freundlich equation is given by:

$$Log\ q_e = \log K_f + \frac{1}{n}\ Log\ C_e \qquad (3)$$

Where K_F (mg/g) and n are the Freundlich constants related to adsorption capacity and intensity, respectively. A linear plot of qe against log Ce will give K_F and n is values. The results of the Langmuir and Freundlich adsorption isotherms plot can be seen in Figure 9.

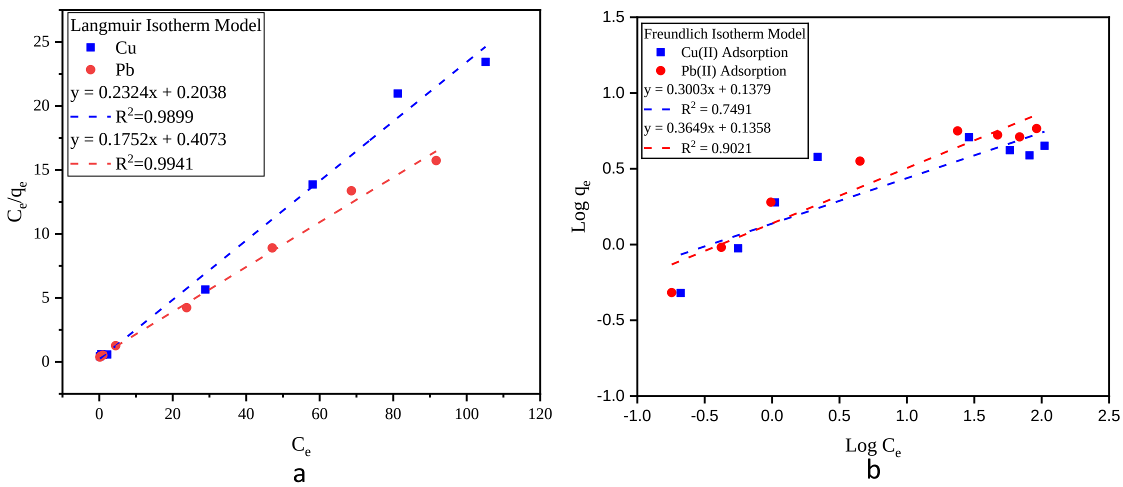

Figure 9. Adsorption isotherm model (a) Langmuir (b) Freundlich.

The equations of the Freundlich and Langmuir isotherms were derived by calculating the values of qe, Ce/qe, Log Ce/qe, and Log Ce, and plotting the graphs by inserting the values of Ce/qe against Ce to obtain the Langmuir equation and inserting Log qe against Log Ce to obtain the Freundlich equation. The Freundlich graph obtained a negative sign due to the very low efficiency value produced. Factors that affect the low efficiency value include the initial concentration of the solution. This also occurred in research using heavy metal concentrations of 5 mg/L [33]. Adsorption is very small at low concentrations but it will increase as the concentration of the solution increases. Testing of the Freundlich and Langmuir adsorption equations was verified with good linearity graphs and having coefficient of determination R^2 values approaching 1. The resulting equation shows that the adsorption of Pb(II) and Cu(II) follows the Langmuir adsorption equation with R^2 values of 0.99 obtained for Pb(II) and 0.98 for Cu(II). This indicates that adsorption occurs in a single layer and the surface is homogeneous. In addition to the R^2 value obtained, the max Q values obtained for Pb and Cu are 58 mg/g and 51 mg/g. Previous research has been conducted using chitin resulting in a Q max of 67 mg/g [34], this strengthens the research on BSF pupal shell as an adsorbent. Another study also used chitin from shrimp shells that can sorb Cr (IV) metal with a maximum Q of 0.97 mg/g [35].

8. Adsorption Kinetic Model

The adsorption kinetics model is determined by plotting the adsorbent capacity adsorbed over time. Factors influencing adsorption kinetics include adsorbent, adsorbate, temperature, and pH. Additionally, agitation speed and particle size can affect adsorption kinetics, where higher agitation speed reduces film thickness and smaller particle size reduces pore diffusion resistance. These factors impact the mass transfer occurring during adsorption [36]. The adsorption reaction kinetics models used in this study are the pseudo-first order (PFO), pseudo-second order (PSO) models and intraparticle diffusion kinetic model.

Determination of adsorption kinetics involves study of the adsorption capacity and kinetic constant values based on varying contact times. Contact time serves as a measure of adsorption rate until equilibrium is achieved. The most suitable kinetics model is determined based on the coefficient of determination, known as R^2 in scientific literature. The R^2 value ranges from 0 to 1, where a higher R^2 indicates a more linear curve based on linear regression. Therefore, an R^2 value closer to 1 indicates better fit [37].

The pseudo-first order kinetics model was introduced by Lagergren in 1898 to describe adsorption kinetics based on solution concentration and adsorption capacity. Generally, the plot of the pseudo-first order kinetics model forms a straight line by plotting the logarithm of (qe - qt) on the y-axis against time (t) in minutes on the x-axis. The pseudo-first order equation is represented in its linear form as:

$$\log(q_e - q_t) = \log q_e - \frac{k_1}{2.303} t \qquad (4)$$

where qe and qt (mg/g) are the amount of metal ion adsorbed at equilibrium and at time t (min), respectively and k_1 is the rate constant of pseudo-first order equation (min^{-1}). The linear plot of log (qe - qt) against t will give k_1 value. The results of the pseudo-first order kinetics model in this study can be seen in Figure 10.

The kinetic analysis of adsorption data continues with determining the simple linear equation of the pseudo-second order (PSO). The pseudo-second order kinetics model was presented by Ho and McKay in 1999 as one of the most popular methods used to fit the adsorption rate data of metal ions, dyes, and other compounds from solution to adsorbents The pseudo-second order equation is represented in its linear form as:

$$\frac{t}{q_t} = \frac{1}{k_2 q_e^2} + \frac{t}{q_e} \qquad (5)$$

where k_2 is the rate constant of pseudo-second order equation (g/(mg min)). The values of qe and k_2 can be determined from linear plot of t/qt against t. The results of the pseudo-second order kinetics model in this study can be seen in Figure 11.

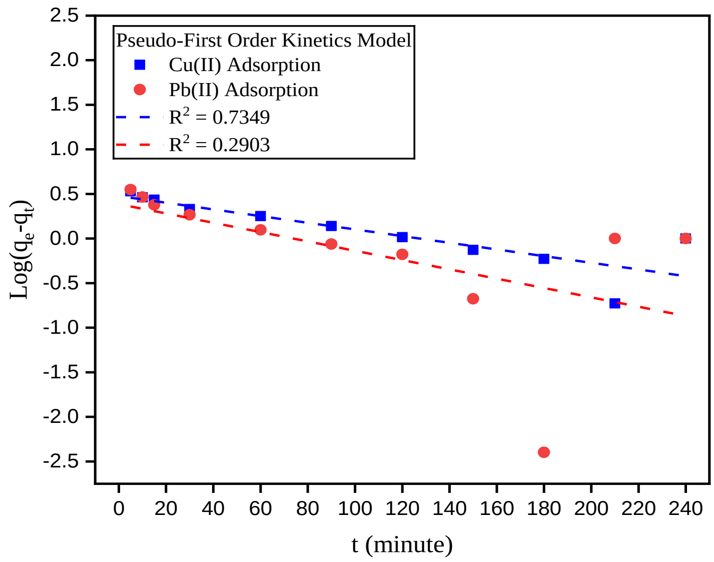

Figure 10. The pseudo-first order kinetics

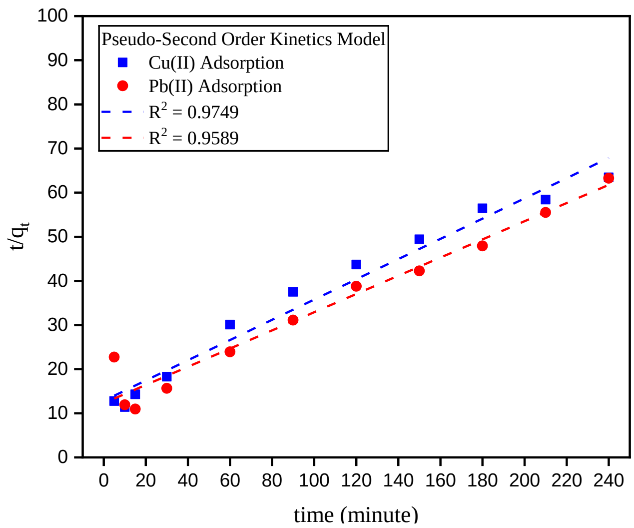

Figure 11. The pseudo-second order kinetics

The results of the analysis comparing the pseudo-first order and pseudo-second order kinetics models to determine the suitable kinetic model are compared by examining the measured parameters from the regression equations, including R^2, k_1, k_2, and qe, as presented in the Table 3. and Table 4.

Table 3. Kinetic Model Parameters for Pb(II) and Cu(II) in PFO.

	Pseudo-First Order		
	R^2	k_1	q_e
Pb(II)	0,29	0,01 min^{-1}	2,43 mg/g
Cu(II)	0.73	0,001 min^{-1}	2,99 mg/g

Table 4. Kinetic Model Parameters for Pb(II) and Cu(II) in PSO.

	Pseudo-Second Order		
	R^2	k_2	q_e
Pb(II)	0,96	0,0035 g/mg/min	4,85 mg/g
Cu(II)	0,97	0,0041 g/mg/min	4,36mg/g

Based on the Table 3., it can be observed that the R^2 value for the pseudo-second order model approaches one and is greater than that of the pseudo-first order model, indicating that the adsorption kinetics suitable for this study is the pseudo-second order model. This is supported by the theory stating that a higher R^2 value indicates a more linear curve and better fit [38]. This research utilizes the pseudo-second order kinetics model, suggesting that in the adsorption chemisorption occurs, involving chemical reactions between the adsorbent and adsorbate. the results of this study are also in line with previous research [39]. Chemical reactions that may occur include ion exchange, surface complexation, and precipitation. This study uses a pseudo second-order kinetics model, which shows that in adsorption chemisorption occurs, which involves a chemical reaction between the adsorbent and adsorbate. this is also reinforced by the results of FTIR and EDX. FTIR results support the appearance of functional groups such as O-H, C-H, and CO_3^{2-}. in EDX results also appear various elements that allow chemisorption to occur. This is reinforced by the larger value of k_1 compared to k_2. A large k_1 value indicates a high adsorption rate due to adsorption diffusion and physical adsorption, while the smaller k_2 value suggests a lower adsorption rate potentially due to chemisorption [40].

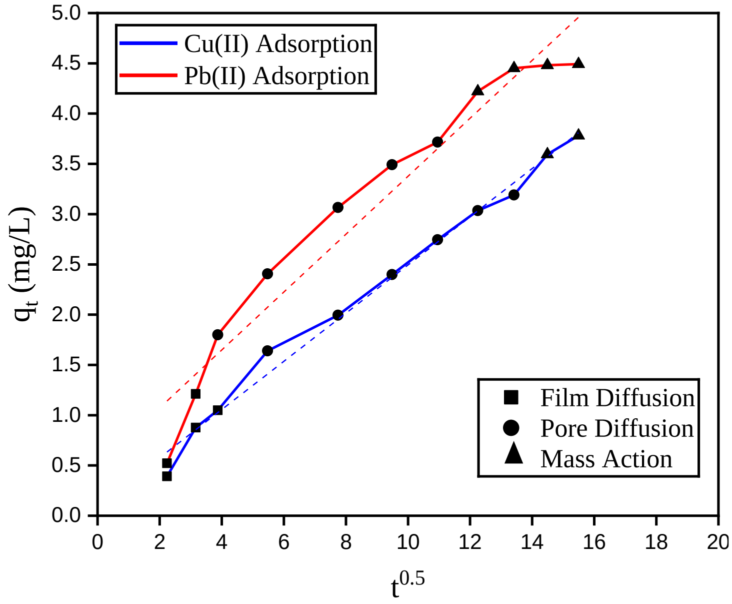

Figure 12. The intraparticle diffusion model

This study has the similar results as other studies using adsorbents based chitin presented in the form of Table 5.

Table 5. Comparison results with another research.

Adsorbent	Parameters	References
Crab shell	R^2_{pfo} = 0.994 R^2_{pso} = 0.986 k_1 = 0.060 k_2 = 0.001 q_{epfo} = 53.1 q_{epso} = 64.47	[41]
Shrimp shell	R^2_{pfo} = 0.947 R^2_{pso} = 0.995 k_1 = 0.016 k_2 = 0.0027 q_{epfo} = 8.56 q_{epso} = 12.85	[42]
Shrimp shell	R^2_{pfo} = 0.91 R^2_{pso} = 0.97 k_1 = 0.06 k_2 = 0.008 q_{epfo} = 12.7 q_{epso} = 13.2	[43]

Meanwhile, the Morris-Weber intraparticle diffusion model equation is commonly used to describe the intraparticle diffusion of solutes under well-agitated conditions, thereby reducing surface diffusion occurrences. The Weber-Morris model is modified to assess the influence of adsorbent surface diffusion based on the resulting constants. Determination of the intraparticle Weber-Morris model involves plotting qt against time ($t^{0,5}$) in minutes to obtain constant values based on the curve slope [44]. This plot results in multilinearity, indicating different stages of adsorption processes. The intraparticle diffusion equation is expressed as:

$$q_t = k_{id} t^{0.5} \quad (6)$$

where kid (mg/(g min$^{-0.5}$)) is the rate constant of intraparticle diffusion equation. The results of the internal diffusion model in this study can be seen in Figure 12.

The internal adsorption diffusion model (intraparticle) shows three main stages that need to be considered to explain the overall process within the intraparticle diffusion model. The first stage indicates film diffusion, while the second stage demonstrates pore diffusion. Pore diffusion is characterized by slower rates due to lower metal ion concentrations and larger pore sizes. Meanwhile, the third stage shows mass action related to the adsorption of metal ions in the inner part of the pores. Determination of these stages is based on the sections of the line produced. A steeply rising line segment represents film diffusion, a gradually rising segment depicts pore diffusion, and a constant or no increase segment indicates mass action [45].

CONCLUSION

Based on the results obtained in this study, the adsorbent exhibits basic chemical characteristics with a pHpzc value of 9.4. FTIR analysis reveals the presence of functional groups indicating the occurrence of chitin and $CaCO_3$ compounds in the BSF pupal shell. SEM-EDX analysis confirms that the adsorbent has a porous morphology characterized by irregular shapes. The optimal pH value determined from this research is 5.5, achieving a high adsorption efficiency of 95.5% for Pb(II) and 71.81% for Cu(II). For Pb(II) adsorption, the optimum contact time is 180 minutes, resulting in an adsorption efficiency of 95.5%. Meanwhile, for Cu(II) adsorption, the optimal contact time is 240 minutes with an efficiency of 94.56%. In terms of concentration, the optimal condition for Pb(II) adsorption is achieved at 20 mg/L, yielding an adsorption efficiency of 95.10%. For Cu(II) adsorption, the optimal concentration is 40 mg/L, resulting in an efficiency of 94.56%. The equations derived from the experimental data fit well with the Langmuir adsorption model, showing high R^2 values of 0.99 for Pb and 0.98 for Cu, indicating excellent correlation between experimental and model-predicted values. Regarding the kinetics of adsorption, the study reveals that the process follows the pseudo-second order kinetic model. This model suggests initial chemical interaction followed by external and internal (intraparticle) diffusion processes, which collectively govern the adsorption kinetics of Pb(II) and Cu(II) on the BSF pupal shell. For the future works, the sudy involved temperature effect and adsorption-desorption cycles (regeneration) should be added. Real wastewater should be tested using prototype of pilot plant. Detail characterization should be completed (moisture, particle analysis, BET analysis).

REFERENCES

[1] A. Yusfaddillah, R. D. Saputri, T. W. Edelwis, dan H. Pardi, “Heavy metal pollution in Indonesian waters,” *BIO Web of Conferences*, vol. 79, p. 04001, 2023. doi: 10.1051/bioconf/20237904001

[2] N. Fahimah, I. R. S. Salami, K. Oginawati, S. H. Susetyo, A. Tambun, A. N. Ardiwinata, dan S. Sukarjo, “The assessment of water quality and human health risk from pollution of chosen heavy metals in the Upstream Citarum River, Indonesia,” *Journal of Water and Land Development*, vol. 56, pp. 153–163, 2023. doi: 10.24425/jwld.2023.143756

[3] S. Rajoria, M. Vashishtha, dan V. K. Sangal, “Treatment of electroplating industry wastewater: a review on the various

techniques," *Environmental Science and Pollution Research*, vol. 29, no. 48, pp. 72196–72246, 2022. doi: 10.1007/s11356-022-18643-y

[4] T. Aragaw, "Chromium Removal from Electroplating Wastewater Using Activated Coffee Husk Carbon," *Adsorption Science & Technology*, vol. 2022, Article ID 7646593, 2022. doi: 10.1155/2022/7646593

[5] L. Weerasundara, Y. S. Ok, dan J. Bundschuh, "Selective Removal Of Arsenic In Water: A Critical Review," *Environmental Pollution*, vol. 268, p. 115668, 2021. doi: 10.1016/j.envpol.2020.115668

[6] M. Uddin dan Y. Jeong, "Efficiently performing periodic elements with modern adsorption technologies for arsenic removal," *Environmental Science and Pollution Research*, vol. 27, no. 32, pp. 39888–39912, 2020. doi: 10.1007/s11356-020-10323-z.

[7] S. Manoj, S. S. Patil, dan M. R. Naik, "Understanding the molecular mechanisms for the enhanced phytoremediation of heavy metals through plant growth promoting rhizobacteria: A review," *Journal of Environmental Management*, vol. 254, p. 109779, 2020. doi: 10.1016/j.jenvman.2019.109779.

[8] J. Thilagan, S. Goplakrishnan, dan T. Kannadasan, "Continuous Fixed Bed Column Adsorption of Copper (II) Ions from Aqueous Solution by Calcium Carbonate," *International Journal of Engineering Research and Technology*, vol. 4, no. 12, pp. 413–418, 2015, doi: 10.17577/IJERTV4IS120456.

[9] Y. D. Ngapa dan J. Gago, "Optimizing of Competitive Adsorption Methylene Blue and Methyl Orange using Natural Zeolite from Ende-Flores," *JKPK (Jurnal Kimia dan Pendidikan Kimia)*, vol. 6, no. 1, pp. 39–48, 2021, doi: 10.20961/jkpk.v6i1.46132.

[10] S. Wahyuni, R. Selvina, R. Fauziyah, H. T. Prakoso, P. Priyono, dan S. Siswanto, "Optimasi Suhu dan Waktu Deasetilasi Kitin Berbasis Selongsong Maggot (Hermetia ilucens) Menjadi Kitosan," *Jurnal Ilmu Pertanian Indonesia*, vol. 25, no. 3, pp. 373–381, 2020. doi: 10.18343/jipi.25.3.373.

[11] A. Waśko, A. Bulak, A. Polak-Berecka, M. Nowakowicz-Dębek, dan A. Bieganowski, "The first report of the physicochemical structure of chitin isolated from Hermetia illucens," *International Journal of Biological Macromolecules*, vol. 92, pp. 316–320, 2016. doi: 10.1016/j.ijbiomac.2016.07.040.

[12] S. Siddiqui, M. R. Khan, dan M. A. Khan, "The potential of chitin and chitosan from dead black soldier fly (BSF) (Hermetia illucens) for biodegradable packaging material–A critical review," *Process Safety and Environmental Protection*, vol. 175, pp. 1–13, 2024. doi: 10.1016/j.psep.2024.01.012.

[13] Y. Lin, Y. Zhang, dan X. Chen, "Sustainable extraction of chitin from spent pupal shell of black soldier fly," *Processes*, vol. 9, no. 6, p. 976, 2021. doi: 10.3390/pr9060976.

[14] T. Hahn, J. Roth, R. Reichl, dan J. Müller, "Purification of chitin from pupal exuviae of the black soldier fly," *Waste and Biomass Valorization*, pp. 1–16, 2022. doi: 10.1007/s12649-022-01678-0.

[15] N. Abidin, M. A. Kamarudin, dan M. A. Zainol, "The potential of insects as alternative sources of chitin: An overview on the chemical method of extraction from various sources," *International Journal of Molecular Sciences*, vol. 21, no. 3, p. 1–25, 2020. doi: 10.3390/ijms21031020.

[16] R. Forutan, M. R. Khosravi, dan M. R. Khosravi, "The first report of the physicochemical structure of chitin isolated from Hermetia illucens," *International Journal of Biological*

Macromolecules, vol. 92, pp. 316–320, 2016. doi: 10.1016/j.ijbiomac.2016.07.040.

[17] N. Jaafarzadeh, M. A. Rahmanian, dan M. R. Khosravi, "Adsorption of Zn(II) from aqueous solution by using chitin extracted from shrimp shells," *Jentashapir Journal of Health Research*, vol. 5, no. 11, pp. 131–139, 2013, doi: 10.22102/jaehr.2014.40151.

[18] Z. Zango, M. R. Khosravi, dan M. R. Khosravi, "A systematic review on applications of biochar and activated carbon derived from biomass as adsorbents for sustainable remediation of antibiotics from pharmaceutical wastewater," *Journal of Water Process Engineering*, vol. 67, p. 106186, 2024. doi: 10.1016/j.jwpe.2024.106186.

[19] A. Labidi, M. R. Khosravi, dan M. R. Khosravi, "Adsorption of copper on chitin-based materials: Kinetic and thermodynamic studies," *Journal of the Taiwan Institute of Chemical Engineers*, vol. 6, no. 1, pp. 140–148, 2016, doi: 10.1016/j.jtice.2016.04.030.

[20] P. Souza, M. R. Khosravi, dan M. R. Khosravi, "Removal of bromophenol blue anionic dye from water using a modified exuviae of Hermetia illucens larvae as biosorbent," *Environmental Monitoring and Assessment*, vol. 192, no. 3, 2020, doi: 10.1007/s10661-020-8110-z.

[21] I. Mandasari dan A. Purnomo, “Penurunan Ion Besi (Fe) dan Mangan (Mn) dalam Air dengan Serbuk Gergaji Kayu Kamper,” *Jurnal Teknik ITS*, vol. 5, no. 1, pp. 1–6, 2016.

[22] N. Bih, et al., “Adsorption of phenol and methylene blue contaminants onto high-performance catalytic activated carbon from biomass residues,”. *Heliyon*, vol. 11, no. 1. 2025, doi: 10.1016/j.heliyon.2024.e41150.

[23] T. M. Thanh *et al*., “Synthesis of iron doped zeolite imidazolate framework-8 and its remazol deep black RGB dye adsorption ability,” *Journal of Chemistry*, vol. 2017, Article ID 5045973, 2017. doi: 10.1155/2017/5045973

[24] A. Aichour dan H. Zaghouane-Boudiaf, “Highly brilliant green removal from wastewater by mesoporous adsorbents: Kinetics, thermodynamics and equilibrium isotherm studies,” *Microchemical Journal*, vol. 146, pp. 1255–1262, 2019. doi: 10.1016/j.microc.2019.02.003

[25] M. Mushtaq *et al*., “Highly brilliant green removal from wastewater by mesoporous adsorbents: Kinetics, thermodynamics and equilibrium isotherm studies,” *Microchemical Journal*, vol. 146, pp. 1255–1262, 2019. doi: 10.1016/j.microc.2019.02.003

[26] B. I. Okolo *et al*., “Adsorption of lead(II) from aqueous solution using Africa elemi seed, mucuna shell and oyster shell as adsorbents and optimization using Box–Behnken design,” *Applied Water Science*, vol. 10, no. 8, pp. 1–23, 2020. doi: 10.1007/s13201-020-01242-y

[27] K. Phiwdang *et al*., “Synthesis of CuO nanoparticles by precipitation method using different precursors,” *Energy Procedia*, vol. 34, pp. 740–745, 2013. doi: 10.1016/j.egypro.2013.06.822

[28] Y. Chuang *et al*., “Sorption studies of Pb(II) onto montmorillonite clay,” *IOP Conference Series: Earth and Environmental Science*, vol. 1087, no. 1, p. 012015, 2022. doi: 10.1088/1755-1315/1087/1/012015

[29] Y.-S. Lin *et al*., “Sustainable extraction of chitin from spent pupal shell of black soldier fly,” *Processes*, vol. 9, no. 6, p. 976, 2021. doi: 10.3390/pr9060976

[30] M. Zhao *et al*., “Preparation of honeycomb-structured activated carbon–zeolite composites from modified fly ash and the adsorptive removal of Pb(II),” *ACS*

Omega, vol. 7, no. 1, pp. 9684–9689, 2022. doi: 10.1021/acsomega.1c07000

[31] S. Kim, J. Lee, dan H. Kim, "Identification of pH-dependent removal mechanisms of lead and arsenic by basic oxygen furnace slag: Relative contribution of precipitation and adsorption," *Journal of Cleaner Production*, vol. 279, p. 123451, 2021. doi: 10.1016/j.jclepro.2020.123451

[32] N. Zainudin, R. I. M. Rashid, A. R. Ishak, dan A. Ali, "Removal of Lead (Pb) From Aqueous Solutions Using Exoskeleton of Black Soldier Fly (BSF)," *Environment-Behaviour Proceedings Journal*, vol. 8, no. 25, pp. 175–184, 2023. doi: 10.21834/ebpj.v8i25.4864

[33] X. Li, L. Xu, J. Gao, M. Yan, H. Bi, dan Q. Wang, "Surface modification of chitin nanofibers with dopamine as efficient nanosorbents for enhanced removal of dye pollution and metal ions," *International Journal of Biological Macromolecules*, vol. 253, p. 127113, 2023. doi: 10.1016/j.ijbiomac.2023.127113

[34] A. Basem, M. A. El-Sayed, dan H. A. El-Sayed, "Adsorption of heavy metals from wastewater by chitosan: A review," *Results in Engineering*, vol. 19, p. 102404, 2024. doi: 10.1016/j.rineng.2023.102404

[35] D. Nasution, R. N. Lubis, dan R. S. Lubis, "Determination of Maximum Adsorption Capacity of Chitosan and Carboxymethyl Chitosan on the Absorption of Metal Ions Cr (VI) Based on the Langmuir Equation," *Journal of Chemical Natural Resources*, vol. 6, no. 1, pp. 30–38, 2024, doi: 10.32734/jcnar.v6i1.16212.

[36] K. L. Tan dan B. H. Hameed, "Insight into the adsorption kinetics models for the removal of contaminants from aqueous solutions," *Journal of the Taiwan Institute of Chemical Engineers*, vol. 74, pp. 25–48, 2017. doi: 10.1016/j.jtice.2017.01.024

[37] D. Chicco, M. J. Warrens, dan G. Jurman, "The coefficient of determination R-squared is more informative than SMAPE, MAE, MAPE, MSE and RMSE in regression analysis evaluation," *PeerJ Computer Science*, vol. 7, p. e623, 2021. doi: 10.7717/peerj-cs.623

[38] A. M. Alwan Al Mashhadani, T. A. Himdan, A. S. Hamadi Al Dulaimi, dan Y. I. M. AbuZaid, "Adsorptive removal of some carbonyl containing compounds from aqueous solutions using Iraqi porcelanite rocks: a kinetic-model study," *Caspian Journal of Environmental Sciences*, vol. 20, no. 1, pp. 117–129, 2022. doi: 10.22124/cjes.2022.5406

[39] P. Rahmania dan A. Bagastyo, "Removal of napthol dye from batik wastewater using chitosan from black soldier fly pupal exuviae," *Analit: Analytical and Environmental Chemistry*, vol. 9, no. 1, pp. 151–163, 2024. Available: https://analit.fmipa.unila.ac.id/index.php/analit/article/view/191.

[40] Y. Chuang, J. Chen, J. Lu, L. Su, S. Y. Jiang, Y. Zhao, C. H. Lee, Z. Wu, dan H. D. Ruan, "Sorption studies of Pb(II) onto montmorillonite clay," *IOP Conference Series: Earth and Environmental Science*, vol. 1087, no. 1, p. 012007, 2022. doi: 10.1088/1755-1315/1087/1/012007

[41] J. Algethami, M. A. Alharthi, M. A. Alshahrani, dan M. A. Alharthi, "Chitin extraction from crab shells and synthesis of chitin@metakaolin composite for efficient amputation of Cr(VI) ions," *Environmental Research*, vol. 252, p. 119065, 2024. doi: 10.1016/j.envres.2021.119065

[42] M. Abomosallam, M. A. Alharthi, M. A. Alshahrani, dan M. A. Alharthi, "Adsorption kinetics and thermodynamics of toxic metal ions onto chitosan nanoparticles extracted from shrimp shells," *Nanotechnology for Environmental Engineering*, vol. 7, pp.

1–13, 2022. doi: 10.1007/s41204-022-00145-2

[43] M. Makhlouf, M. A. Alharthi, M. A. Alshahrani, dan M. A. Alharthi, "Eco-friendly synthesis of biosorbent based on chitosan-activated carbon/zinc oxide nanoparticle beads for efficiency reduction of cadmium ions in wastewater," *Biomass Conversion and Biorefinery*, pp. 1–16, 2024. doi: 10.1007/s13399-024-04567-2

[44] A. A. Alwan Al Mashhadani, T. A. Himdan, A. S. Hamadi Al Dulaimi, dan Y. I. M. AbuZaid, "Adsorptive removal of some carbonyl containing compounds from aqueous solutions using Iraqi porcelanite rocks: a kinetic-model study," *Caspian Journal of Environmental Sciences*, vol. 20, no. 1, pp. 117–129, 2022. doi: 10.22124/cjes.2022.5406

[45] A. Tomczyk, M. S. Sokołowska, dan M. Boguta, "Biomass type effect on biochar surface characteristic and adsorption capacity relative to silver and copper," *Fuel*, vol. 278, p. 118183, 2020. doi: 10.1016/j.fuel.2020.118183